B.F.A. van Hest, H.F. Groenen & D.M. Passchier

Nonlinear Development and Breakdown of TS-waves in an Adverse Pressure Gradient Boundary Layer

Abstract

The *natural* transition process in boundary layers subjected to an adverse pressure gradient (APG) and low free stream turbulence intensities has been studied experimentally using hot-wire anemometry. The initial growth of Tollmien-Schlichting waves is shown to agree with linear stability theory. The TS-wave amplitude distribution across the boundary layer shows two near-wall maxima. The nonlinear development of the Tollmien-Schlichting waves is shown to be of a combined resonance, with fundamental resonance observed at the first near-wall maximum and subharmonic resonance at the second maximum. Breakdown to turbulence occurs at the second near-wall maximum. The streamwise intermittency distribution is found to follow Narasimha's universal intermittency distribution, while Klebanoff's fit in normal direction needs a modification.

Introduction

The transition from laminar to turbulent boundary layer flow, subject to small free stream disturbances, begins with the generation of instability waves, known as Tollmien-Schlichting waves, in the boundary layer. After a region of exponential growth the waves reach a finite amplitude and nonlinear processes set in. These processes lead to a local breakdown of the flow and the formation of turbulent spots. The length of the transition region is determined by the growth rate of the turbulent spots.

Although linear amplification and subsequent nonlinear processes have been verified extensively for zero pressure gradient (ZPG) flow (see e.g. Klingmann *et al.*, 1993 and Kachanov & Levchenko, 1984), stability data for flow with adverse pressure gradients is still scarce. Recent experiments (Gostelow *et al.*, 1995, van Hest *et al.*, 1995) have shown that an adverse pressure gradient dramatically increases the spot growth rates.

This paper presents the later stages of development and subsequent breakdown of natural TS-waves in a low-speed boundary layer with adverse pressure gradient. We will focus on the growth of the TS-waves and their sub- and higher harmonics, the break-down position and the subsequent growth of turbulent spots in the transition region. The obtained experimental data can be used

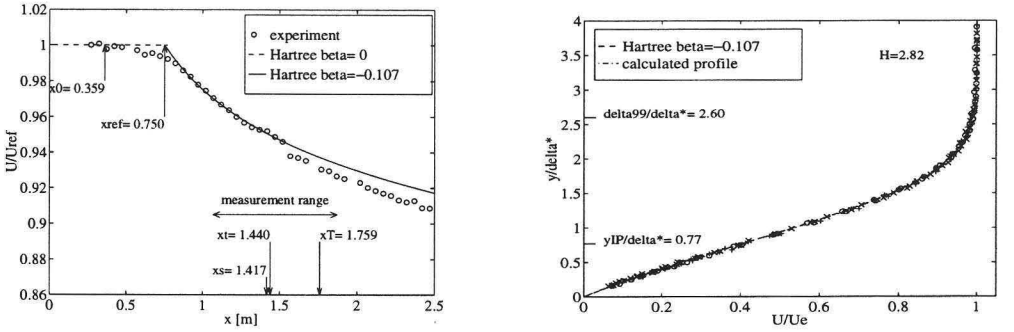

Figure 1: Comparison between measured and Hartree $\beta = -0.10$ pressure distribution (left). Measured and Hartree $\beta = -0.10$ velocity profiles (right).

to develop more accurate models for the prediction of the transition onset and transition length of boundary layers along aircraft fuselage and wings.

Experimental procedure

The measurements were conducted on the flat test wall of a closed return wind tunnel. Different pressure gradients can be imposed by the flexible wall opposite of the test wall. The imposed pressure gradient (Fig. 1 left) varied from nearly neutral over the first 0.75 m, to Hartree $\beta = -0.107$ further downstream. The laminar velocity profiles (Fig. 1 right), measured in between $1.070 \leq x \leq 1.320$ m, have a shape factor $H = 2.82 \pm 0.04$, which corresponds to a Falkner-Skan profile with $\beta = -0.107$. The reference velocity was $U_{ref} = 10$ m/s, measured at $x_{ref} = 0.27$ m, and the free stream turbulence level was $Tu = 0.09$ %.

Velocity measurements were performed with Constant Temperature Anemometers with both single and cross hot-wires. At each position at least 1.2×10^5 samples, depending on the local turbulence intensity in the boundary layer, were taken at a sampling rate of $f_s = 4000$ Hz.

Tollmien-Schlichting wave development

Linear growth

The power spectral density was calculated from the discrete time series of the fluctuating velocity signal using the Fast Fourier Transform algorithm and the Welch averaging method. The power spectral density $P(f)$ is defined such that

$$\overline{u^2} = \int_0^\infty P(f)df. \tag{1}$$

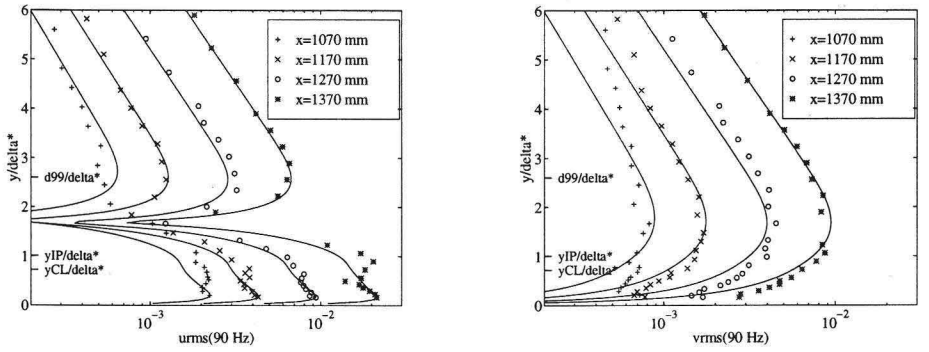

Figure 2: Measured and calculated TS-wave amplitude distributions at four streamwise positions in the frequency band of the most amplified TS-wave.

The velocity spectra showed a broad maximum in the frequency range between 50 and 130 Hz, with three discrete peaks (probably caused by larger initial background disturbances) at $f = 69$ Hz, $f = 90$ Hz and $f = 109$ Hz. This frequency range corresponds to the most amplified Tollmien-Schlichting waves according to linear stability theory. In the remainder of this paper, we will consider only the central maximum at $f = 90$ Hz. The development of the amplitude distribution of the streamwise and normal velocity fluctuations in the frequency band 90 ± 2 Hz is presented in Fig. 2. All the experimental amplitude distributions of the streamwise component of fluctuating velocity show a second near-wall maximum located at $y/\delta^* \approx 0.9$ (close to the critical layer and the inflexion point in the velocity profile). This second near-wall maximum is not present in the eigen functions calculated on the basis of linear stability theory (shown by the solid lines). In an earlier experiment with an APG boundary layer (see Wubben *et al.*, 1990), it was suggested that the second maximum was due to the effect of nonlinear interactions but no supporting evidence was given. Linear stability calculations for oblique Tollmien-Schlichting waves (Rist, 1996) show that three-dimensional TS-waves have a maximum at the position of the second near-wall maximum. Therefore, the experiments suggest that both two-dimensional and three-dimensional Tollmien-Schlichting waves are present in our flow at the same time.

The amplitude growth of the TS-wave and its subharmonic and higher harmonics were followed in the streamwise direction at the height of the first and second near-wall maxima (see Fig. 3). The growth of the TS-waves at both near-wall maxima agrees well with linear stability theory (solid line) up to $x = 1.320$ m, which is approximately two TS-wavelengths upstream of the onset of transition. At the first maximum both the subharmonic and second harmonic grow rapidly downstream of $x = 1.220$ m, where the rms-value in the 90 Hz-frequency band has an amplitude of 0.1 % of the edge velocity. At the second maximum, the subharmonic grows continuously from the first measurement position at $x = 1.070$ m with an enhanced growth downstream of $x = 1.270$ m (where

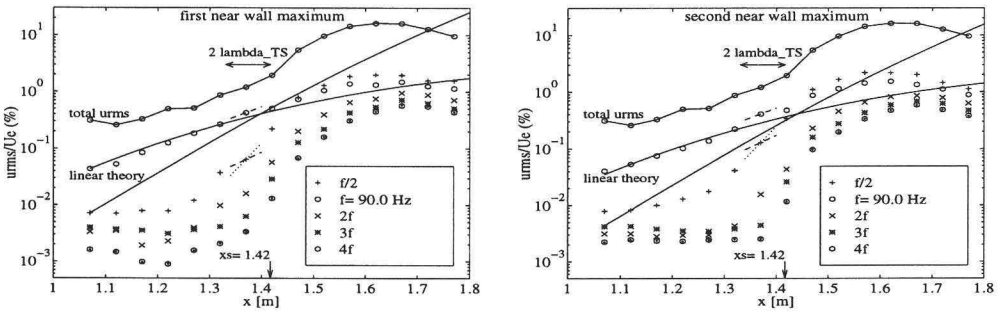

Figure 3: Amplitude of the subharmonic, fundamental and higher harmonics at the first near-wall maximum (left) and second near-wall maximum (right).

$u_{rms}(90\text{ Hz})/U_e = 0.1\ \%$). Although the subharmonic modes are unstable, their amplification rate is much smaller than predicted by linear theory (solid line). Secondary instability calculations for subharmonic resonance (Rist, 1996) performed for a 2D base profile and 2D eigenfunctions with $A_{rms}/U_e = 0.7\ \%$ (at $x = 1.370\ m$) and oblique subharmonic waves with $\phi = 60°$ provide the correct growth rate (dotted line). It must be noted, however, that the actual propagation angle of the oblique subharmonic waves in this experiment is unknown.

Tollmien-Schlichting wave resonance

Nonlinear interactions between Tollmien-Schlichting waves with the fundamental frequency and oblique subharmonics or oblique fundamental waves can be regarded as a form of three-wave interaction which causes a constant phase difference between the waves involved. As the present experiment considers natural Tollmien-Schlichting wave growth, in contrast with vibrating-ribbon experiments, there is no direct method to determine whether a constant phase difference between the different frequencies exists. Therefore, the use of bispectral analysis (see Corke, 1987) has been adopted to determine nonlinear interactions between different waves. The bispectrum $B_u(f_1, f_2)$ is defined as

$$B_u(f_1, f_2) \;=\; E\left[\tilde{u}(f_1)\tilde{u}(f_2)\tilde{u}^*(f_1 + f_2)\right], \tag{2}$$

with $\tilde{u}(f)$ the Fourier transform, $\tilde{u}^*(f)$ its complex conjugate and $E[\ ]$ the expectation operator. Because the velocity signal is a real signal and auto-bispectra are calculated, a number of symmetry relations can be used to reduce the frequency plane for which the bispectrum is calculated to the area given by

$$\begin{array}{lll} 0 & \leq f_2 & \leq \frac{1}{4} f_s \\ f_2 & \leq f_1 + f_2 & \leq \frac{1}{2} f_s - f_2. \end{array} \tag{3}$$

The physical interpretation of the bispectrum is that it measures the degree of energy-transfer between to waves of frequencies f_1 and f_2, by which a third wave is generated with the sum or difference frequency $f_3 = f_1 \pm f_2$. Because the amplitude of the Tollmien-Schlichting waves, and as a consequence the absolute value of the energy transfer, changes in streamwise direction it is more interesting to determine the normalized bispectrum, called the bicoherence spectrum or bicoherence. The bicoherence is defined as a measure for the degree of phase locking between two waves.

$$b_u^2(f_1, f_2) = \frac{|B_u(f_1, f_2)|^2}{E\left[|\tilde{u}(f_1)\tilde{u}(f_2)|^2\right] E\left[|\tilde{u}^*(f_1 + f_2)|^2\right]}, \tag{4}$$

with $0 \leq b_u^2 \leq 1$. A bicoherence of one indicates a quadratic interaction between a frequency pair (f_1, f_2), resulting in a third wave with sum or difference frequency f_3. For values in between zero and one a partial interaction takes place, which means that part of the waves with frequency f_3 are caused by the quadratic interaction, whereas the rest are spontaneous oscillations. A value of zero at a frequency pair (f_1, f_2) means that no phase relationship between those frequencies is present. Because of the presence of noise in experimental signals, the bicoherence will always be in the range between zero and one. We will speak of quadratic interactions when the bicoherence lies above the mean noise level plus one standard deviation in the noise level, which is calculated in a part of the frequency plane without interactions. We will present the bicoherence spectra, with the frequency f_1 fixed (at the Tollmien-Schlichting frequency and its sub- or higher harmonic), as a function of the second frequency f_2.

Special attention must be given to interpreting the bicoherence spectra. When a high bicoherence is observed at (f_1, f_2), three possible interactions could have taken place, namely (i) the sum or difference frequency results from the interaction between f_1 and f_2, (ii) f_1 interacts with the sum or difference frequency to give f_2, or (iii) f_1 is the result of interaction between f_2 and the sum or difference frequency. When the origin of a mode is known, like in the present case where the TS-frequency is known from linear stability theory and frequency spectra, this is not a problem. In other cases the order of interacting frequencies has to be determined from the streamwise development of the bicoherence.

From $x = 1.270$ m to 1.420 m the bicoherence spectra (see Fig. 4) show a phase locking between the fundamental frequency $f_1 = 90$ Hz and its harmonics f_1, $2f_1$, $3f_1$, etc at the first near-wall maximum. Further, a resonance is found between two of the three discrete frequencies in the velocity spectra, i.e. interactions between $f_1 = 90$ Hz and $f_2 = 69$ Hz take also place. These interactions produce high levels of bicoherence at (f_1, f_2), $(f_1 + f_2, f_2)$ and $(2f_1, f_2)$. A subharmonic resonance is displayed at the second maximum. At the first streamwise position, the same interactions are found as in the case of the fundamental resonance. Further downstream, maxima in the bicoherence appear at $(\frac{1}{2}f_1, \frac{1}{2}f_1)$, $(\frac{1}{2}f_2, \frac{1}{2}f_2)$ and at $(f_1 - f_2, \frac{1}{2}f_2)$ and $(f_1 - f_2, \frac{1}{2}f_1)$. One TS-wavelength before breakdown, the bicoherence becomes larger at higher frequencies up to approxi-

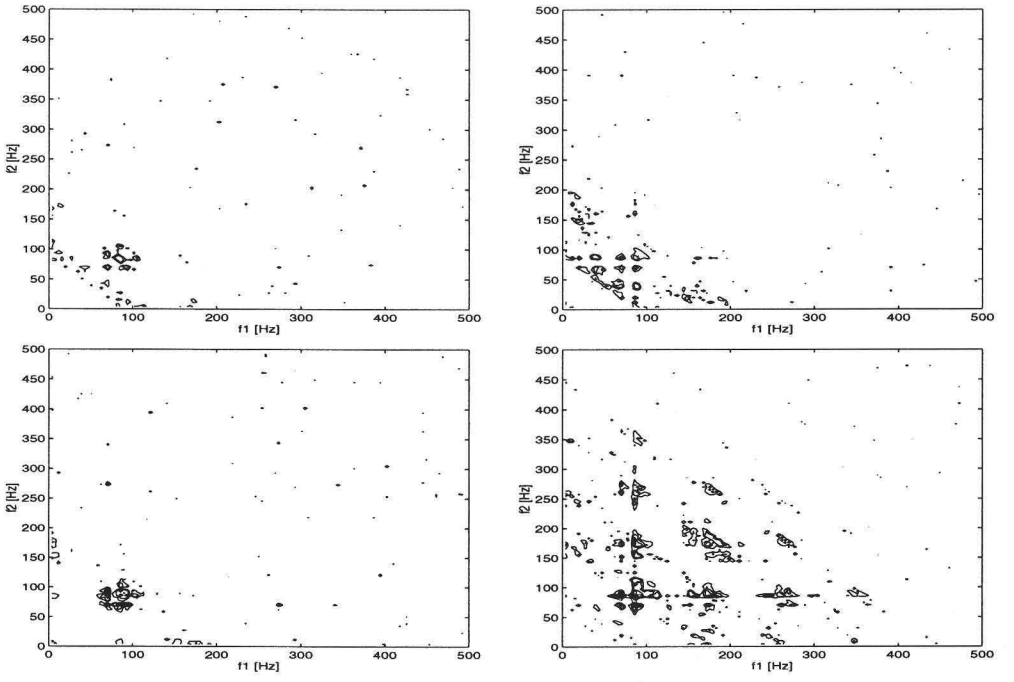

Figure 4: Streamwise development of the bicoherence spectra at the second (upper graphs) and first (lower graphs) near-wall maximum, at $\Delta x = 2\lambda_{TS}$ and $\Delta x = \lambda_{TS}$ upstream of transition onset and at transition onset.

mately $4f_1$. In the transition region the bicoherence continues to spread to higher frequencies but the absolute value of the bicoherence is reduced drastically, first at the lowest frequencies and next for the complete frequency domain.

From the above mentioned results we believe that the measured secondary instability of the TS-waves is of a mixed type, in which both the higher harmonics and subharmonics are amplified through a phase-locking mechanism. This mechanism differs for different positions in the boundary layer.

Breakdown and intermittency

At $x = 1.420\ m$ the TS waves break up and natural turbulent spots appear at approximately the height of the inflexion point. The turbulent spots were detected by comparing a *detection function*, taken as the short time average of $|d^2u/dt^2|$, with a threshold level. Next, the velocity record was divided into laminar and turbulent regions. The fraction of time that the flow is turbulent, i.e. the intermittency γ, is shown in Fig. 5 left across the boundary layer. Klebanoff (1956) presents the following fit to the intermittency distribution for

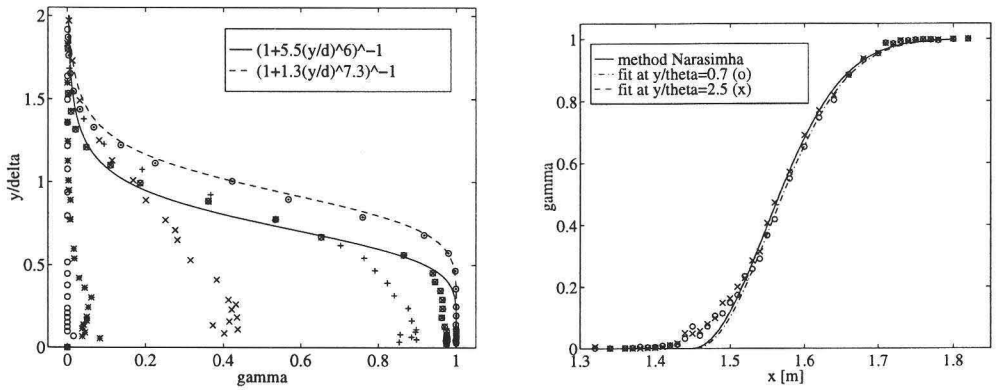

Figure 5: Intermittency distribution across the boundary layer (left graph) in the transition region and initial turbulent boundary layer at $x = 1.370(\bigcirc)$, $x = 1.470(*)$, $x = 1.570(\times)$, $x = 1.670(+)$, $x = 1.770(\otimes)$ and $x = 1.870\ m(\odot)$. Intermittency in streamwise direction (right graph), measured at two wall distances ($y/\delta^* = 0.2$ & $y/\delta^* = 0.9$).

(*fully developed*) ZPG turbulent boundary layers

$$\gamma(y) = \left[1 + c_1 \left(\frac{y}{\delta}\right)^{c_2}\right]^{-1}, \tag{5}$$

with $c_1 = 5.5$ and $c_2 = 6$. A modification is necessary to fit this relation to our APG *turbulent* boundary layer (at the, last, *turbulent* stations). New values are given by $c_1 = 1.3$ and $c_2 = 7.3$. It must be remarked that these values depend on the definition of the boundary layer thickness (which is not given by Klebanoff). A second explanation for the difference may be the short distance between the turbulent stations and the end of transition.

Through the transition region the intermittency increases from zero at onset to one in the turbulent boundary layer (shown in Fig. 5 right at the wall distance of the two near-wall maxima in the Tollmien-Schlichting wave amplitude distribution). The curve follows the 'universal' intermittency distribution as proposed by Narasimha, except at the beginning, which is possibly due to the large negative spikes in the velocity signal prior to breakdown. This gives high values of $|d^2u/dt^2|$ and therefore causes an early detection of small patches of 'turbulence'. Narasimha's 'universal' intermittency distribution is given by

$$\gamma(x) = 1 - \exp\left[-n_t\sigma\frac{(x - x_t)^2}{U_e}\right], \tag{6}$$

with $n_t\sigma = 0.411\frac{U_e}{\lambda^2}$, x_t the start of transition and $\lambda = x_{\gamma=0.75} - x_{\gamma=0.25}$ a characteristic parameter for the length of the transition region. A fit of equation 6 to the experimental data with $n_t\sigma$ given by a relation for the spot formation

and growth, $n_t\sigma = n_t \tan\alpha(U_e/U_{te} - U_e/U_{le})$ (see Chen & Thyson, 1971), results in a spot formation rate $n_t = 1.05 \times 10^3$, a spanwise growth $\alpha = 16.5°$ and trailing edge velocity[1] $U_{te}/U_e = 0.38$. These values agree well with results from a triggered turbulent spot experiment with the same local pressure gradient (see van Hest, 1995). This result gives confidence in models for the length of the transition region based on experiments with triggered turbulent spots.

Conclusions

- Linear stability theory provides a good prediction of TS-wave growth.
- In the present experiments both 2D and 3D TS-waves seem to be present in the flow, resulting in measured TS-wave amplitude distributions with two near-wall maxima.
- Phase-locking between fundamental and higher harmonics and between fundamental and subharmonics is observed respectively at the first and second near-wall maxima of the TS-wave amplitude distribution.
- Breakdown to turbulence occurs at the second near-wall maximum.
- The normal intermittency distribution in APG flow needs a modification compared to Klebanoff's definition. This may depend on either the definition of the boundary layer thickness or the 'state-of-development' of the turbulent boundary layer.
- The streamwise intermittency distribution agrees with Narasimha's universal distribution. A fit to the experimental intermittency provides spot propagation parameters in agreement with triggered spot experiments.

References

Chen, K.K. & Thyson, N.A. 1971 – Extension of Emmons' spot theory to blunt bodies, *AIAA* **9**, 821-825.

Corke, T.C. 1987 – Measurements of resonant phase locking in unstable axisymetric jets and boundary layers, *Non-linear Wave Interactions in Fluids*, volume 87 of *AMD*, 37-65.

Gostelow, J.P., Melwani, N., Solomon, W.J., & Walker, G.J. 1995 – Effects of a self-similar adverse pressure distribution on turbulent spot development, *AIAA* **95-2254**.

Hest, B.F.A. van, Passchier, D.M., & van Ingen, J.L. 1995 – The development of a turbulent spot in an adverse pressure gradient boundary layer, IUTAM symposium *Laminar-Turbulent Transition* Sendai, Japan, pp. 255-262.

Kachanov, Y.S. & Levchenko, V.Y. 1984 – The resonant interaction of disturbances at laminar-turbulent transition, *J. Fluid Mech.* **138**, 209-247.

[1]It has been shown that the leading edge velocity ($U_{le}/U_e = 0.89$) is almost constant.

Klebanoff, P.S. 1956 – Characteristics of turbulence in a boundary layer with zero pressure gradient, NACA *Technical Report* TN 3178.

Klingmann, B.G.B., Boiko, A.V., Westin, K.J.A., Kozlov, V.V. & Alfredsson, P.H. 1993 – Experiments on the stability of Tollmien-Schlichting waves, *Eur.J.Mech., B/Fluids* **12**, 493-514.

Rist, U. 1996 private communication, Universität Stuttgart, Germany.

Wubben, F.J.M., Passchier, D.M. & van Ingen, J.L. 1990 – An experimental investigation of Tollmien-Schlichting instabilities in an adverse pressure gradient boundary layer, IUTAM Symposium *Laminar-Turbulent Transition* Toulouse, France, 31-42.

Authors' address

Delft University of Technology
Faculty of Aerospace Engineering
Kluyverweg 1
2629 HS Delft, The Netherlands